Geoderma 285 (2017) 164–172

Contents lists available at ScienceDirect

Geoderma

journal homepage: www.elsevier.com/locate/geoderma

Disappearance and alteration process of charcoal fragments in cumulative soils studied using Raman spectroscopy

Jun Inoue [a,*], Ayaka Yoshie [a], Takeshi Tanaka [b], Takeshi Onji [b], Yohtaro Inoue [b]

[a] Department of Geosciences, Osaka City University, 3-3-138 Sugimoto, Sumiyosi-ku, Osaka 558-8585, Japan
[b] Technology Research Institute of Osaka Prefecture, 2-7-1 Ayumino, Izumi 594-1157, Japan

ARTICLE INFO

Article history:
Received 24 May 2016
Received in revised form 22 September 2016
Accepted 26 September 2016
Available online 10 October 2016

Keywords:
Carbonization
Graphitization
Degradation
Black carbon
Biochar

ABSTRACT

Raman spectra of charcoal fragments in cumulative soils in central Japan, where grasslands have been sustained using intentional burning for ~1000 years, were obtained and compared to those of fresh charcoal fragments after modern grass burning to clarify their disappearance and alteration process in the soils. Although the values of each Raman-spectrum parameter of the soil charcoal and fresh charcoal fragments are partially similar, certain differences indicating their alteration or disappearance were observed. Charcoal fragments with lower graphitization in soils altered chemically with age at decadal to century scale, suggested by changes in distance between defects or defect type of their chemical structures. Charcoal fragments with higher graphitization were found in fresh charcoal samples, whereas very few charcoal fragments were found in both young and old soils, indicating that these charcoal fragments disappeared instantly after they were formed. This fact implies that charcoal fragments with higher graphitization tend to not remain in soils, possibly owing to their physical properties such as fragility, density, and hydrodynamic behavior. Our findings suggest that charcoal's physical properties have a vital influence on charcoal residues in soils, as do charcoal's chemical properties.

1. Introduction

Charcoals are produced from plant combustion such as forest fires, grassland fires, and other fires. Charcoals can be utilized by putting them in soils for several purposes, e.g., soil improvement, pollutant immobilization, and carbon sequestration, so-called "biochar" (Jeffery et al., 2015). Because charcoal has a polyaromatic structure, in general, it is thought to be much more chemically stable than other organic materials (Deluca and Boisvenue, 2012; Haumaier and Zech, 1995; Santin et al., 2015; Schmidt et al., 2011). Therefore, charcoal in soils or sediments could contribute to a major atmospheric carbon sink or slow-cycling carbon pools (Lehmann et al., 2006; Masiello, 2004; Preston and Schmidt, 2006). However, the stability of charcoal in soils is yet to be elucidated, although the stability of the charcoal has been examined and discussed for decades. This is because the chemical and physical properties of charcoals vary widely depending on the thermal condition and their precursors, and their stability could be different owing to the difference of their properties (Antal and Grønli, 2003; Ascough et al., 2008; Bergeron et al., 2013; Bourke et al., 2007; de Lafontaine and Asselin, 2012; Gundale and Deluca, 2006; Kasin and Ohlson, 2013; Keiluweit et al., 2010; Nichols et al., 2000; Ohlson, 2012; Santin et al., 2015; Scott, 2000; Scott and Jones, 1994; Spokas, 2010). These previous studies show that higher charring temperatures generally result in charcoals with higher carbon content and more polyaromatic structures, which would be a higher recalcitrant to chemical attack such as oxidation (Ascough et al., 2010, 2011). Even in a single fire (e.g., forest fire or grassland fire), the thermal conditions are spatially different and the material varies in terms of plant species and organs, resulting in charcoal fragments with various chemical properties (Ohlson, 2012; Scott and Jones, 1994; Scott et al., 2000). Therefore, even a single fire produces charcoal fragments with variations in their stability.

Recent studies have examined the alteration of charcoal or charcoal fragments in soils or sediments in various ways and these studies indicate that charcoal fragments possibly altered over time through both biotic and abiotic mechanisms in soils (Ascough et al., 2011; Bird et al., 1999; Braadbaart et al., 2009; Cheng et al., 2006; Inoue and Inoue, 2009; Kasin and Ohlson, 2013; Sultana et al., 2010; Nishimura et al., 2012; Steinbeiss et al., 2009; Zimmerman, 2010). Most of the studies examined masses of charcoal fragments in soils to clarify their chemical properties, and some studies compared these fragments to freshly produced charcoal fragments. These studies have contributed to further understanding the degradation process of charcoal fragments in soils. As mentioned above, however, the stability of charcoals varies widely depending on the thermal conditions and materials, suggesting that examination of respective charcoal fragments is necessarily to evaluate the degradation of charcoal fragments in soils in detail. Raman spectroscopy (using visible or infra-red excitation) has become an important

* Corresponding author.
E-mail address: juni@sci.osaka-cu.ac.jp (J. Inoue).

http://dx.doi.org/10.1016/j.geoderma.2016.09.032

technique for characterizing materials, especially those with rich sp^2 carbon structures. The technique has also been adapted to examine thermal alteration or carbonization processes of plant materials (Ascough et al., 2010; Francioso et al., 2011; Ishimaru et al., 2007; Kawakami et al., 2005; McDonald-Wharry et al., 2013; Smith et al., 2016; Yamauchi and Kurimoto, 2003; Zickler et al., 2006). As Raman spectroscopy is very sensitive to alteration of the carbon structure, the technique would also contribute to the evaluation of the degradation of charcoals in soils. Furthermore, the spectra can be acquired on small areas, enabling the evaluation of the carbonization and alteration of respective charcoal fragments.

Here, we examine the carbon structures of respective charcoal fragments in cumulative soils in central Japan using Raman spectroscopy to evaluate the alteration of the charcoal fragments. The cumulative soils have deposited for over several thousands of years, where the Japanese-pampas grassland has been burned intentionally and distributed for ~1000 years. The history of the intentional burning and grassland development was reconstructed from phytolith assemblages, charcoal concentrations, and radiocarbon dating of the cumulative soils (Okunaka et al., 2012) and palynological data obtained from lacustrine sediments nearby (Inoue et al., 2012). In this study, we used charcoal fragments extracted from soil samples dated to after 1000 years ago. We also examined fresh charcoal fragments produced after modern grassland fires in the area and compared parameters of the Raman spectra of soil charcoal and fresh charcoal to clarify the alteration process of charcoal fragments in the cumulative soils. The profiles of soils and charcoal fragments reconstructed paleoecologically would provide a meaningful context to clarify the alteration process in the area, because the context confirms that the precursors and thermal condition of the charcoal fragments in the soils are similar to those of fresh charcoal found after present-day grassland fires. The facts indicate that, in this area, the chemical properties and structure of soil charcoal fragments were originally similar to those of fresh charcoal fragments. Thus, the differences of the parameters of the Raman spectra between soil charcoal and fresh charcoal imply the influences of charcoal alteration or other processes on the cumulative soils.

2. Materials and methods

2.1. Study site and soil charcoal samples

For Raman spectra analysis of soil charcoals, we used soil samples collected from the Soni plateau in central Japan. The plateau is covered with grassland, dominated by *Miscanthus sinensis* (Japanese pampas grass) and locally covered by *Sasa nipponica* (a kind of dwarf bamboo). The grassland is burnt intentionally every year to enhance its survival. Okunaka et al. (2012) reconstructed the history of intentional fires and grassland developments by phytolith analysis and charcoal analysis (charcoal concentrations) of cumulative soils distributed on the plateau; the beginning of intentional fires and grassland developments dates back at least ~1000 years ago and intentional fires and grassland developments have continued until the present day. In the current study, we examined the soil samples collected by Okunaka et al. (2012). The samples have been preserved in a refrigerator (at 5 °C).

The soils of the Soni plateau are characterized by a thick (up to 70 cm) black high-humic A-horizon that is loosely compact, classified as Andisols, as indicated on a soil map (Nara Prefecture, 1973, 1986; Okunaka et al., 2012). The detailed soil descriptions and radiocarbon ages are shown in Okunaka et al. (2012), implying that the soils developed upward, i.e., they are cumulative soils. For Raman spectra analysis, we used soil samples of 0–3 cm and 14–25 cm depths in the A-horizon from the soil profile at Site 1 (34°31′10″N, 136°09′45″E) in Okunaka et al. (2012). The reason for selection of these samples is that these soils include a large number of charcoal fragments (>1000 fragments per cm^{-3} of soil) certainly developed under the grasslands by intentional fire, as shown in Okunaka et al. (2012). Radiocarbon dating of the age of humin (including charcoal fragments) and humic acids in the soil samples at 14–25 cm and 3–14 cm depths is 693–910 years before present (cal BP) and 0 cal BP, respectively. This suggests that the charcoal fragments in the soil samples at 14–25 cm were produced around 800 years ago and those at 0–3 cm depth were produced in modern times (probably, at most 100 years ago).

To extract charcoal fragments from the soil samples and remove humic acid, fulvic acid, and carbonate from the charcoal fragments, we treated the samples as follows. First, the soil samples were treated with 1.5 M KOH solution for 24 h, and then >125 μm fragments were collected using a sieve with a 125 μm mesh size. The fragments were placed in the 1.5 M KOH solution for 24 h. After washing the fragments well with pure water, the fragments were placed in 1.0 M HCl solution for 24 h. Then the fragments were washed and placed in pure water for 1 h. After that, we collected 125–250 μm fragments using sieves of 125 and 250 μm mesh sizes for Raman spectra analysis. During each treatment, the solutions containing fragments were stirred slowly (~70 rpm) using a magnetic stirrer, and room temperature was maintained at approximately 25 °C using an air conditioner. The reasons that 125–250 μm fragments were selected for Raman spectra analysis is that all fragments in this size range can be discriminated with certainty between charcoal fragments and other fragments using a microscope, and the soil samples used in this study have a large number of charcoal fragments <250 μm.

2.2. Fresh charcoal samples

Fresh charcoal samples were collected right after intentional burning on the Soni plateau on March 21, 2015 (Fig. 1). To obtain a representative fresh charcoal sample, 8 sites were selected to collect charcoal samples, and the sites were at a distance of 50–200 m from each other. Charcoal samples were collected in areas of several hundreds of cm^2 at each site and preserved in stainless steel cups (Fig. 1). All the charcoal in these samples was broken up into fragments (less than ~1 cm length) by using scissors. Charcoal fragments with a mass of 0.1 g were taken from each sample and mixed together, and the charcoal fragments in the mixed sample were then crushed into smaller fragments. These small charcoal fragments were gently washed through nested sieves (mesh sizes: 125 and 250 μm) to yield 125–250 μm fragments similar to the soil charcoal samples. For Raman spectrum analysis, the fresh charcoal samples were subjected to the same chemical treatments as the soil samples.

2.3. Raman spectra analysis

For Raman spectra analysis of the charcoal fragments, charcoal selection was restricted to fragments that were silky, black, completely opaque, and angular under a microscope. The appearance of the charcoal fragments in the soil samples was similar to that of the fresh charcoal fragments (Fig. 2).

Raman spectra were acquired with a NRS-3300 Raman spectrometer (Jasco) equipped with a cooled CCD detector, which is housed at the Technology Research Institute of Osaka Prefecture. A 532 nm green laser was adopted as the excitation source and was focused to a beam approximately 3 μm in diameter at a power of 1–1.5 mW at the sample surface. Data points were recorded at 1 cm^{-1} intervals between 100 and 3900 cm^{-1}. The Raman measurements were performed at four points on each charcoal fragment. For analysis we avoided areas with adherent mineral particles on charcoal fragments. We measured the Raman spectrum of 100 charcoal fragments in each sample. The spectra obtained were modified and each parameter of the Raman spectrum was defined by referring to McDonald-Wharry et al. (2013) as follows (Fig. 3). First, each spectrum was digitally smoothed using a 15 cm^{-1} moving mean before measuring the parameters. A photoluminescence background slope was calculated using linear regression through the data points on the smoothed spectra between 700 and 2000 cm^{-1} while excluding

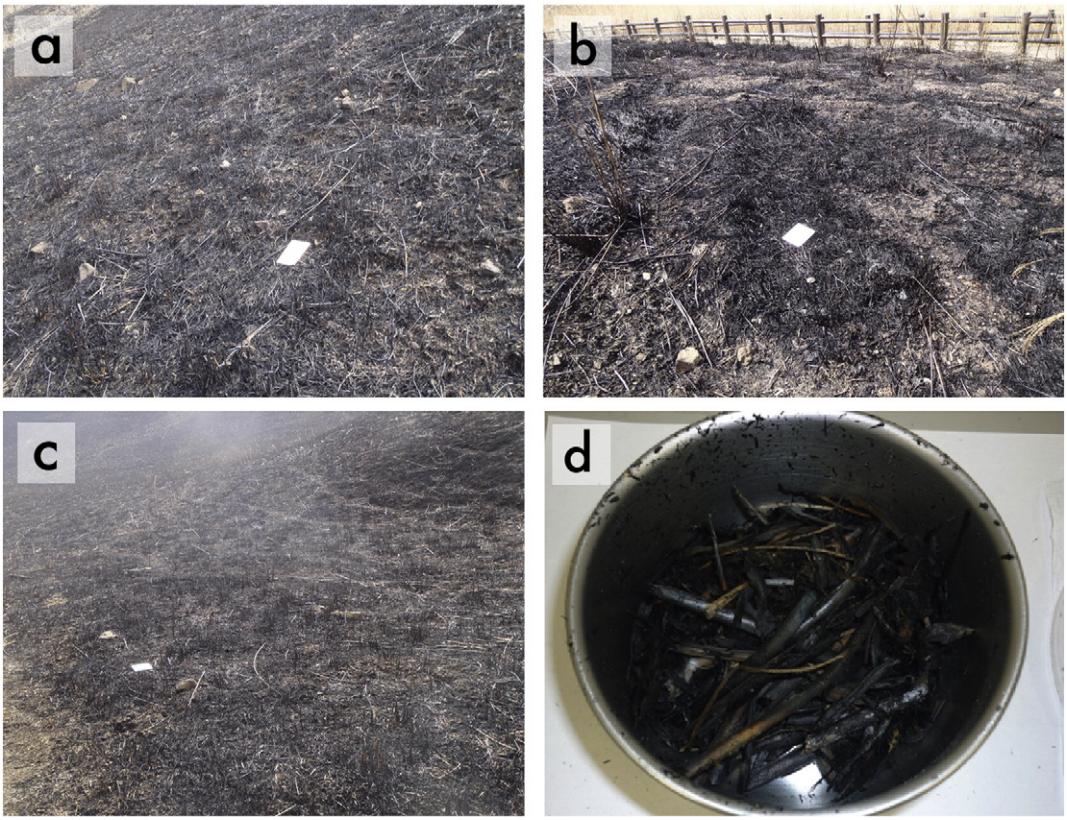

Fig. 1. (a–c) Charcoal distributions at some sites from where we collected samples after intentional grassland fire in the Soni plateau, central Japan, March 21, 2015. (d) Charcoal in a stainless steel cup we collected at a site after the intentional grassland fire.

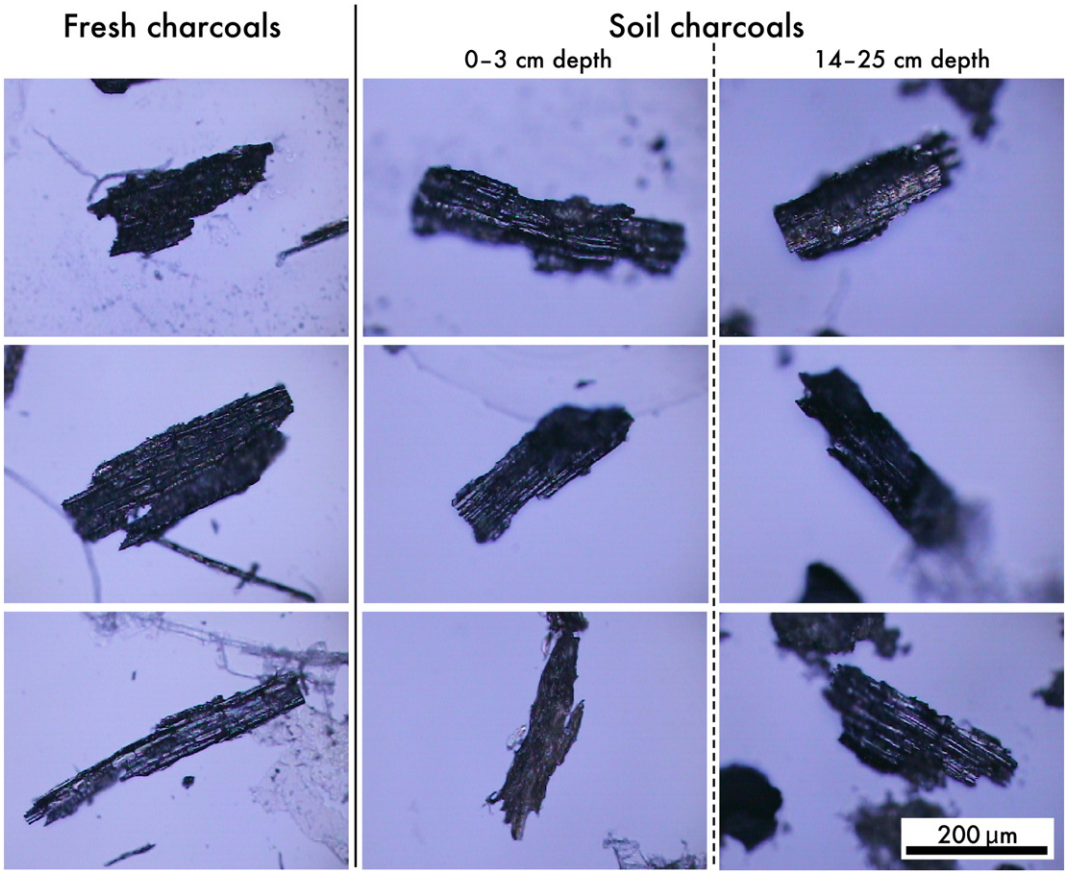

Fig. 2. Appearance of fresh charcoal fragments, charcoal fragments in 0–3 cm depth soil (young soils), and those in 14–25 cm depth soils (old soils) under incident light using a microscope.

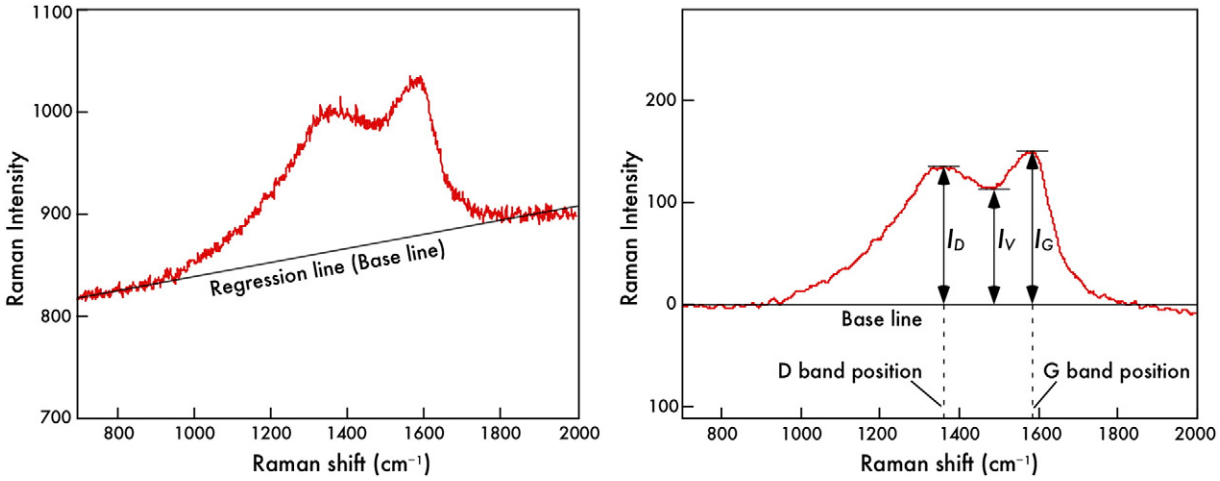

Fig. 3. An example of a raw Raman spectrum (left) and the modified spectrum (right) to obtain the parameters according to the procedure described by McDonald-Wharry et al. (2013). A regression line slope is a photoluminescence background slope. The modified spectrum was obtained after smoothing the raw spectrum with the 15 cm^{-1} moving mean, and the regression line values were subtracted from the smoothed spectrum.

all the data points between 1000 and 1700 cm^{-1}. To obtain the value of each parameter, the regression line values were subtracted from the smoothed spectrum. G band position was measured at the maximum intensity between 1450 and 1700 cm^{-1}, and G band height (I_G) was measured as the maximum intensity in that range. D band position was measured at the maximum intensity between 1210 and 1410 cm^{-1}, and D band height (I_D) was measured as the maximum intensity in that range. The height of the valley (I_V) between the G band and the D band positions was measured as the minimum intensity between 1400 and 1550 cm^{-1}. Following McDonald-Wharry et al. (2013), the parameters of I_D/I_G, I_V/I_G, and the photoluminescence slope/I_G were calculated. The slope of the photoluminescence background line was divided by the G band height (I_G) and then multiplied by 10,000 μm/cm to give a value in μm. For each fragment, the means of each Raman spectra parameter obtained on four data points were calculated.

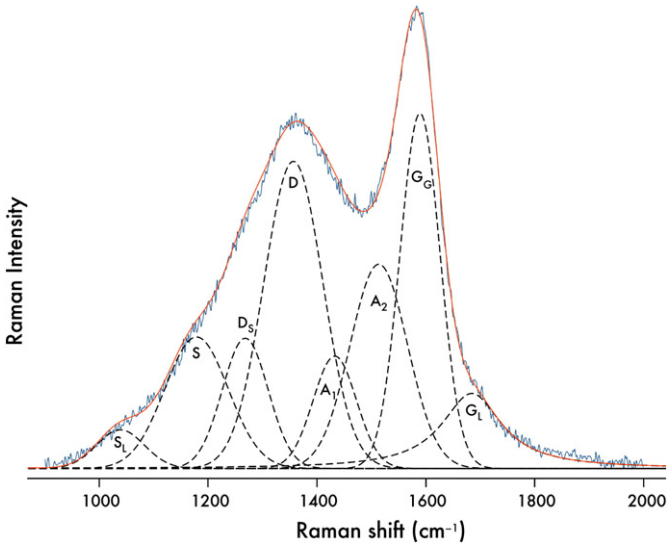

Fig. 4. Deconvolution of the Raman spectra of a fresh charcoal fragment after a modern grassland fire, referring to Smith et al. (2016). Red line indicates a summation of curves, and solid blue line represents the original experimental intensity from the background. Dotted black lines represent the assigned curves.

To assess how the I_D/I_G and I_V/I_G parameters represent the original Raman spectrum peaks, a deconvolution of the Raman spectra of 50 modern charcoal fragments was conducted (Fig. 4). For the deconvolution of the Raman spectra, we used the peak fit tool in MagicPlot ver. 2.7 (Magic Plot Systems, LLC). A version of the software (MagicPlot Student) is available as a free download (http://magicplot.com). Referring to Smith et al. (2016), we deconvoluted the Raman spectra following the procedure below.

1. The spectrum between 900 cm^{-1} and 2000 cm^{-1} was used for the deconvolution. A linear background correction was employed using the minimum intensity between 900 and 1000 cm^{-1} and 1800 and 2200 cm^{-1} as anchor points. We subtracted the background value from each value of the spectrum between 900 and 2000 cm^{-1}, and the values (intensities) were used to find the fitting curves.
2. The values (positions and intensities) were imported into MagicPlot, and the spectrum line was drawn. The Gaussian and Lorentzian curves were added, and their peaks were placed on the local maxima near 1350 cm^{-1} and 1600 cm^{-1}, respectively. Next, the data were fit via a sum of the curves. The "minimum deviation of residual sum of squares," and "maximum number of iterations" were set to 1E-9 and 10,000, respectively. The settings were fixed for "fit the data by sum of curves" for all steps.
3. A new Gaussian curve was subsequently added. The values of the amplitudes and the x-position of the Lorentzian curve were imported to those of the new Gaussian curve (each value was copied and pasted). Then, the Lorentzian curve was deleted. The half width at half maximum (HWHM) of the curve with its peak near 1350 cm^{-1} was set to 60, and the HWHM of the curve with its peak near 1600 cm^{-1} was set to 50. These curves were the preliminary D and G_G peaks, respectively.
4. Other peaks were added, and the values (amplitude, x-position, HWHM) of each peak were set as follows: S_L (0, 1025, 60), S (0, 1175, 60), Ds (0, 1275, 60), A_1 (0, 1430, 60), A_2 (0, 1515, 60), and G_L (50, 1650, 50). All curves were Gaussian-type curves, except for G_L, which was a Lorentzian-type curve.
5. All values (amplitude, x-position, and HWHM) of D, G_G, and G_L were locked. In addition, the x-position and HWHM of the others were locked (the amplitudes were unlocked). Then, the data were fit via a sum of the curves to establish all the preliminary curves.
6. The amplitude and x-position of all curves were locked (the HWHMs were unlocked), except the G_L curve, wherein all values were locked. Then, the data were fit via a sum of the curves to determine their HWHM values.

7. The amplitude and HWHM of all curves were locked (their x-positions were unlocked), except the G_L curve, wherein all values were locked. Then, the data were fit via a sum of the curves to determine their x-position values.
8. The values of all curves were locked, except the G_G and G_L curves, wherein all values were unlocked. Then, the data were fit via a sum of the curves to determine all the values of these curves.

We deconvoluted 50 Raman spectra of fresh charcoal fragments following this procedure, and their coefficients of determination (adjusted R^2) were 0.996–0.998. The peaks of the deconvoluted spectra were generally in the positions summarized by Smith et al. (2016).

3. Results

The Raman spectra parameters of the G band position, D band position, I_D/I_G, I_V/I_G, and the photoluminescence slope/I_G of soil charcoal and fresh charcoal samples are shown in Fig. 5. Yamauchi and Kurimoto (2003) and McDonald-Wharry et al. (2013) showed that the G band position blueshifts with increase in charring temperature. Furthermore, McDonald-Wharry et al. (2013) showed that I_V/I_G and the photoluminescence slope/I_G decrease with increases in charring temperature, especially at lower temperatures (<700 °C). Because the G band positions correlate well with the thermal conditions at low temperatures (<800 °C) independent of the precursors (McDonald-Wharry et al., 2013; Yamauchi and Kurimoto, 2003), here, we adapted the G band position as a standard parameter. In Fig. 5, the horizontal axis denotes the G band positions and the vertical axis denote other parameters. The values of the photoluminescence slope/I_G are on a logarithmic scale, because this parameter has been reported to exponentially increase with hydrogen content when using visible light excitation (Adamopoulos et al., 2004; Buijnsters et al., 2009; Casiraghi et al., 2005; Ferrari and Robertson, 2004; McDonald-Wharry et al., 2013).

Although the ranges of each Raman spectra parameter in each sample are partially similar to each other, the distribution of the parameter values have some differences, e.g., in Fig. 5a, fresh charcoal is dominant

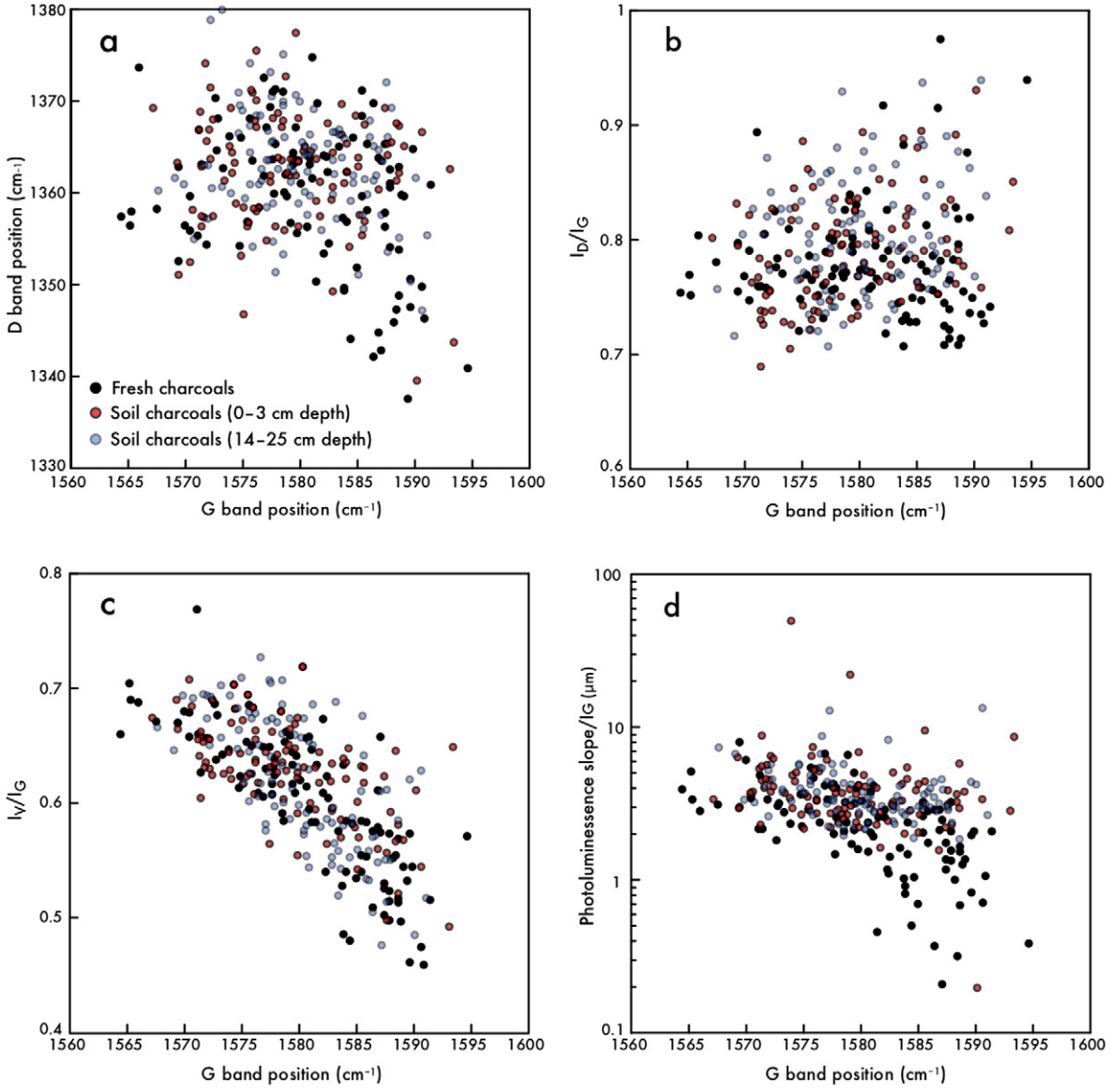

Fig. 5. Raman spectrum parameters obtained from fresh charcoal fragments and soil charcoal fragments (0–3 cm depth and 14–25 cm depth, respectively) according to the procedure described by McDonald-Wharry et al. (2013); G band position (horizontal axes) with (a) D band position; (b) I_D/I_G (intensity height ratios between the D band and the G band); (c) I_V/I_G (height intensity ratios between the valley and the G band); (d) photoluminescence slope/I_G (ratios between the photoluminescence background slope of the Raman spectrum and the intensity height of the G band).

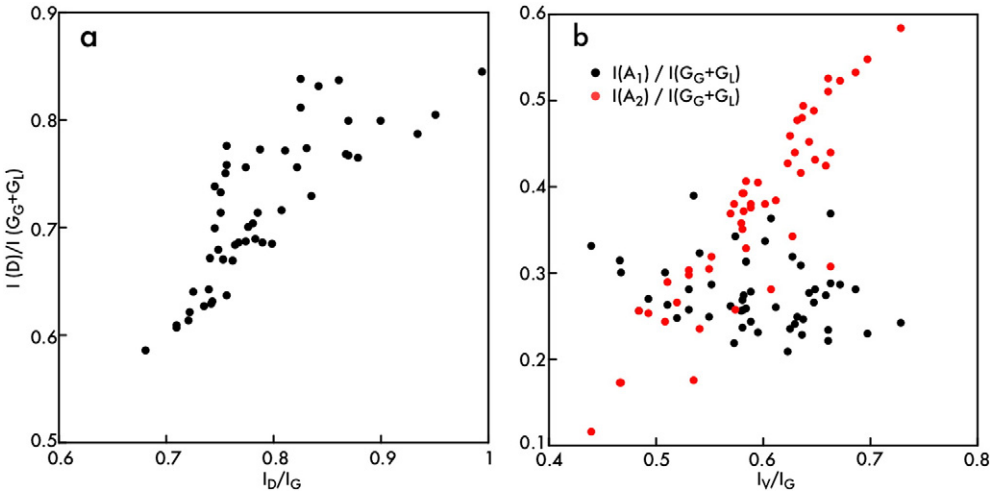

Fig. 6. Relation between the peak intensities of the experimental raw data of Raman spectra and those of the curves assigned from the deconvolution of spectra. The spectra were obtained from fresh charcoal. (a) I_D/I_G versus $I(D)/I(G_G + G_L)$, the ratios between the assigned D peak intensity height and the sum of the intensity heights of assigned G_G and G_L curves. (b) I_V/I_G versus $I(A_1)/I(G_G + G_L)$ or $I(A_2)/I(G_G + G_L)$, the ratios between the assigned A_1 or A_2 peak intensity heights and the sum of the intensity heights of assigned G_G and G_L curves.

in the area of lower D position (<1350 nm) with higher G position (>1585 nm); in Fig. 5d, fresh charcoal is dominant in the area of lower photoluminescence slope/I_G (<~1) with higher G position (>1585 nm).

Fig. 6a shows the relation between I_D/I_G and $I(D)/I(G_G + G_L)$ (the ratio between the peak intensities or the sum of the peak intensities) of 50 deconvoluted Raman spectra of modern charcoal fragments, and Fig. 6b shows the relation between I_V/I_G and $I(A_1)/I(G_G + G_L)$ and $I(A_2)/I(G_G + G_L)$. I_D/I_G correlates strongly with $I(D)/I(G_G + G_L)$ ($R = 0.80$), indicating that I_D/I_G predominantly represents $I(D)/I(G_G + G_L)$, particularly the intensity ratios between I(D) and $I(G_G)$. This is because the intensities of the G_G peaks are generally much higher than those of the G_L peaks. I_V/I_G is closely related to $I(A_2)/I(G_G + G_L)$ ($R = 0.90$), whereas there is no relation between I_V/I_G and $I(A_1)/I(G_G + G_L)$ ($R = -0.24$). This suggests that the change in I_V/I_G primarily represents changes in the ratios of the A_2 intensity to the G_G intensity.

4. Discussion

4.1. Interpretations of each Raman parameter for fresh charcoal

To interpret the Raman parameters of fresh charcoal, a factor analysis was applied to the parameters (the G band position, the D band position, I_D/I_G, I_V/I_G, and the photoluminescence slope/I_G) of the fresh charcoal fragments. Each eigenvalue of Factors 1 and 2 was >1. The components of Factors 1 and 2 are shown in Fig. 7. Factor 1 shows a strong positive loading for the G band position and moderate to strong negative loadings for I_V/I_G, the photoluminescence slope/I_G, and the D band position. Factor 2 shows positive moderate to strong loadings for I_D/I_G and I_V/I_G.

The G band position has a strong positive loading for Factor 1. Previous studies (McDonald-Wharry et al., 2013; Yamauchi and Kurimoto, 2003) indicate that the wavenumber of the G positions generally increases (blueshifts) with increasing charring temperature and that the G positions are strongly correlated with the thermal conditions (primarily the heating temperature) at low temperatures (<800 °C) independent of the precursor. I_V/I_G, the photoluminescence slope/I_G, and the D band position are also predominantly dependent on the thermal conditions. In addition, temperatures in Japanese grassland fires are generally below 800 °C (Iwanami, 1972), and the heating duration of the fire in the study area was likely several to tens of minutes. Therefore, Factor 1 (the horizontal axis in Fig. 6) primarily represents the thermal conditions, in particular the heating temperature, when the fresh charcoal was produced. Changes in the G band position could represent the formation of larger, less distorted ring systems with the removal of the oxygen functional group, sp^3 bonding, and other defects, as the heating temperature increased (McDonald-Wharry et al., 2013; Smith et al., 2016).

In contrast, the I_V/I_G has a strong negative loading for Factor 1, indicating that the I_V/I_G decrease with increasing charring temperature. This is consistent with the finding that I_V/I_G is largely dependent on the charring temperature, as suggested by McDonald-Wharry et al. (2013). The decrease in I_V/I_G with increasing temperature is likely due to the removal of oxygenated defects. This is because I_V/I_G primarily represents the A_2 intensity, as mentioned above, and based on their computational simulations of the relation between Raman spectra and molecule structures, Smith et al. (2016) suggest that oxygenated defects contribute to the intensity of the A_2 region. The photoluminescence slope/I_G for charcoal represents the hydrogen content in the C–H groups, not the hydrogen content in the C–OH functional groups (McDonald-Wharry et al., 2013). Therefore, the negative loading of Factor 1 likely represents the additional removal of C–H groups with increasing temperature.

The D band position also has a moderate negative loading on Factor 1. The wavenumber of the D band positions generally decreases (redshifts) with increasing charring temperature (McDonald-Wharry et al., 2013; Smith et al., 2016). This decrease is thought to be related to the

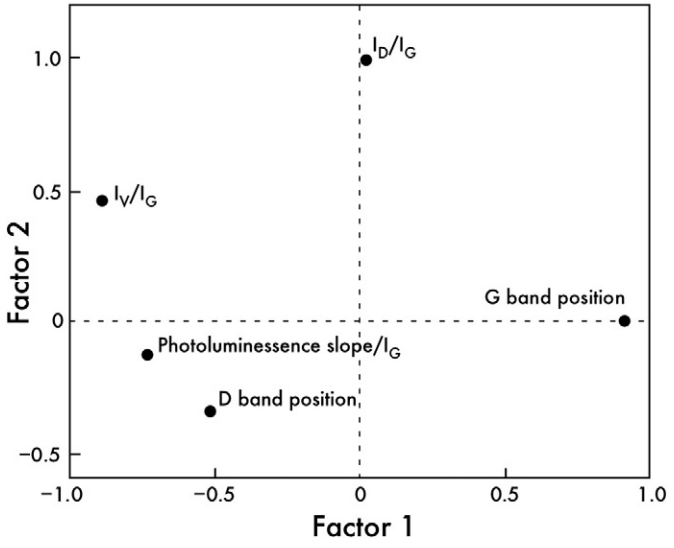

Fig. 7. The factor loading of each parameter estimated from the factor analysis of parameters in the Raman spectra of 100 fresh charcoal fragments.

removal of sp^3 bonded amorphous structures with increasing temperatures resulting in graphite or graphene-like structures that have sp^2 bonded edges terminated with radicals, hydrogen, and oxygen functional groups and/or various edge-reconstructions (McDonald-Wharry et al., 2013).

As mentioned above, the I_D/I_G height ratios have a strong positive loading on Factor 2. The G band peak is due to the bond stretching of all pairs of sp^2 atoms in both rings and chains, whereas the D band peak is due to the breathing modes of the sp^2 atoms in rings (Ferrari and Robertson, 2004; McDonald-Wharry et al., 2013). Even though, for certain precursors, the I_D/I_G height ratios generally increase with increasing charring temperatures (McDonald-Wharry et al., 2013; Smith et al., 2016), the values of I_D/I_G vary significantly depending on the precursor, especially below 700 °C (McDonald-Wharry et al., 2013). Based on the relation between the carbon structure and the G band position suggested in Ferrari and Robertson (2004), because the G positions of the fresh charcoal in this study are between ~1570 and ~1590 nm (Fig. 4), this charcoal is likely composed of nanocrystalline graphite and amorphous carbon. On the carbon structure of the fresh charcoal, the I_D/I_G height ratios are related to the in-plane crystallite graphite size and/or the average distance between defects (McDonald-Wharry et al., 2013). Because the chemical structures of plants can significantly vary, depending on their organs (e.g., their compositions and types of cellulose, hemicellulose, and lignin) and because the precursors of fresh charcoal fragments in this study are also varied, we assume that Factor 2 primarily represents the differences in the precursors of the charcoal fragments via the in-plane crystallite graphite size and/or the distance between defects in those fragments with low carbonization degrees (under the low temperature and/or short heating duration of the grassland fire at the study site). In addition, the defect type and edge type of the structure are likely related to Factor 2, which is likely dependent on the precursor under low carbonization, as suggested by Smith et al. (2016); that is, the spectrum peak's intensity and position differs according to the defect and edge types. These assumptions are consistent with I_V/I_G having a moderate positive loading on Factor 2 because I_V primarily results from oxygenated defects, as discussed above.

4.2. Disappearance and alteration process of charcoal fragments in the soils

Assuming that the distributions of each Raman spectrum parameter of the soil charcoal samples are originally similar to the fresh charcoal, the scores of Factors 1 and 2 for each charcoal fragment (those collected after the modern fire, those in the young soils, and those in the old soils) were calculated to assess the alteration process of the charcoal fragments in soil with time. In the calculations, we used the loading of each parameter for the factor analysis in Fig. 7. Over a quarter (26%) of the fresh charcoal fragments had high Factor 1 scores exceeding 2, whereas very few soil charcoal fragments (2%) had such high scores (Fig. 8). For Factor 2, 16% of fresh charcoal had high scores exceeding 1, and 25% of charcoal in young soils and 30% of charcoal in old soils had high scores (Fig. 8).

The high Factor 1 scores of some fresh charcoal fragments but very few soil charcoal fragments imply that these fresh charcoal fragments were carbonized at high temperatures, and were not significantly included in the soils at the study sites. This is because Factor 1 primarily represents the thermal conditions, as mentioned in the previous section. The very few soil charcoal fragments produced at high temperatures indicate that these charcoal fragments generally tend to alter or disappear soon after they are formed because, even in young soils formed in the last few decades, such fragments are under-represented. Charcoal produced at higher temperatures is generally more chemically stable than that produced at lower temperatures (Ascough et al., 2010, 2011) because higher charring temperatures result in highly graphitic or polyaromatic microcrystalline domains within charcoal microstructures (Cohen-Ofri et al., 2006; Darmstadt et al., 2000). This suggests that charcoal produced under high temperatures, found primarily in fresh charcoal samples, is chemically stable and has not been altered significantly. Therefore, we assume that charcoal fragments produced at high temperature disappear nearly instantly (they are neither altered nor chemically degraded) after they are formed or that the soils initially contain none or few of these charcoal fragments. The thermal conditions (especially the charring temperature and duration) when the charcoal forms generally determine not only the charcoal's chemical properties but also its physical properties, such as its density, reflectance, fragility, pore space, surface area, and hydrodynamic behavior (Bourke et al., 2007; Bustin and Guo, 1999; Chia et al., 2015; Crawford and Belcher, 2014; Gundale and DeLuca, 2006; Jones et al., 1991; Keiluweit et al., 2010; Nichols et al., 2000; Scott and Jones, 1994). Nichols et al. (2000) demonstrated that the waterlogging time of charcoal when it floats on water is dependent on its charring temperature. In addition, Rumpel et al. (2006) showed that charcoal (black carbon) is more prone to removal from soils than other organic matter, and Rumpel et al. (2015) suggested that different soil-charcoal types (biochar types) could be affected differently by water erosion processes. Therefore, charcoal fragments formed at different temperatures could be separated by water flow. Furthermore, the fragility (or abrasion) of charcoal is dependent on the thermal conditions (Crawford and Belcher, 2014; Nichols et al., 2000); the fragility likely increases with increasing charring temperature (Scott, 2010). This is probably because higher charring temperatures result in higher percentages of pore space in charcoal (Chia et al., 2015; Gundale and Deluca, 2006; Keiluweit et al., 2010; Yu et al., 2006), more micro-cracks in the cell

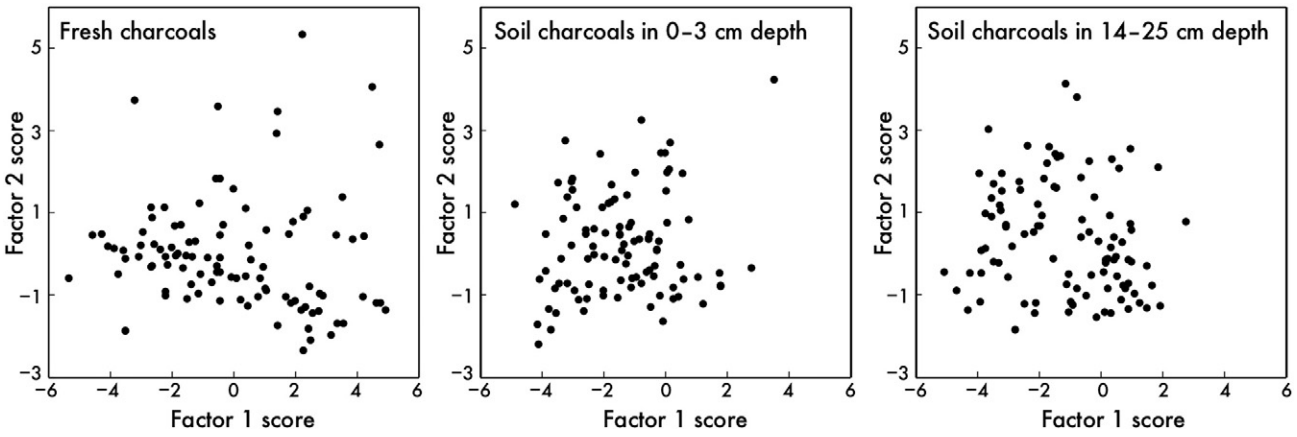

Fig. 8. Factor scores for fresh charcoal, soil charcoal at 0–3 cm depth (young charcoal), and soil charcoal at 14–25 cm depth (old charcoal) calculated from factor loadings in Fig. 7 and parameters in Fig. 5, assuming that the distributions of each Raman spectrum parameter of soil charcoal fragments were originally similar to fresh charcoal. Exceptional scores for very few charcoals are shown in Supplementary data.

structures of charcoal (McParland et al., 2007; Scott and Jones, 1991), and more graphene-like domains since some layers of the graphene-like domains are held together by weak Van der Waals forces. These physical properties of charcoal fragments, which depend on the thermal conditions, influence the residue rate of the charcoal fragments in soils relative to whole charcoal fragments produced from a fire. Therefore, we assume that the disappearance of high-temperature charcoal fragments is due to their fragility or a characteristic of their hydrodynamic behavior; that is, after these charcoal fragments were formed, they were physically broken down and/or swept away by rainwater.

The charcoal fragments in some Japanese Andisols have a reflectance that is small or not >2%; however, in Japan, some charcoal fragments made by grass and forest fires have higher reflectance (Inoue and Inoue, 2009; Nishimura et al., 2012). The difference between the reflectance of soil charcoal and fresh charcoal is not due to alterations via chemical processes because the reflectance is strongly dependent on the thermal conditions. The reflectance generally increases with charring temperature (Bustin and Guo, 1999; Jones et al., 1991; Scott and Jones, 1991), and the original reflectance is retained even after exposure to highly oxidizing conditions (Ascough et al., 2010). This suggests that charcoal fragments with high reflectance disappeared from the soils or disappeared prior to being buried in the soils, which is consistent with our assumption.

For Factor 2, excluding the charcoal fragments with Factor 1 scores >2, even though the means of the scores were not different, as shown by a *t*-test yielding *p*-values > 0.1, the percentages of high scores >1 were different, as mentioned above. Furthermore, the percentages of charcoal with high Factor 2 scores increased with charcoal age in the soils, and these differences could imply the alteration of the charcoal in the soils at the study site. As mentioned above, Factor 2 represents the in-plane crystallite graphite size and/or the distance between defects in the charcoal fragments, and/or a difference in the defect and edge types under low degrees of carbonization. Because the crystallite graphite size is assumed to alter little over short periods of time, the difference in the Factor 2 scores likely represents an alteration in the distance between defects in those fragments (i.e., the area of the defects) and/or the defect and edge types of the chemical structure of the charcoal fragments. Therefore, the changes in the scores suggest an increase in the distance between defects and/or a change in the defect and edge types in the charcoal fragments, i.e., a chemical alteration of the charcoal. Changes in the Factor 2 scores between fresh charcoal and charcoal in young soils is more marked than that between charcoal in young soils and old soils, even though the number of elapsed years is much shorter. This is likely because the biotic activity and weathering in the surface soils is stronger than that in the deep soils. This implies that, at the study site, the chemical alteration of the soil charcoal could occur over decades or centuries.

5. Conclusion

Differences in Raman spectra among fresh charcoal fragments and soil charcoal fragments in old and young soils indicate the alteration or disappearance of charcoal fragments in cumulative soils. Some alteration of charcoal fragments with lower graphitization occurred in the soils, as indicated by the spectrum differences of charcoal fragments among fresh charcoals and charcoals in young and old soils. Most charcoal fragments with higher graphitization were probably broken down or blown out owing to their physical properties, implied by the spectrum differences between fresh charcoal fragments and soil charcoal fragments. We assume that charcoal fragments with more graphene-like domains (produced under higher temperatures) are more chemically stable but less physically stable, resulting in their lower rate of residue as fragments in soils. This possibly applies more to grass-charcoal fragments than woody-charcoal fragments, because grass has no woody component and its components are generally fragile. However, our findings suggest that we should focus on not only charcoal's chemical properties but also its physical properties when we estimate the residue of charcoal fragments in soils. These results suggest that examining respective charcoal fragments in soils by use of Raman spectra could contribute to the evaluation of the alteration or disappearance of charcoals.

Exact evaluations of the degradation and disappearance of charcoal fragments are also important to clarify the fire history from the charcoal concentrations or fluxes in cumulative soils (e.g., Inoue et al., 2016). Furthermore, charcoal in soils could be a major atmospheric carbon sink, for which stability would be an important factor in the estimation of the carbon cycle related to soil charcoals. Therefore, our suggestion possibly contributes to not only soil science but also other fields related to soil charcoal.

Acknowledgments

We thank Dr. Nishimura M. for his cooperation to bring the authors together in the beginning of this study. We also thank Dr. Mitamura M. for his valuable advice. This work was partly supported by Grants-in-Aid for Scientific Research from the Ministry of Education, Culture, Sports, Science and Technology of Japan (No. 16K07646 to J. Inoue).

Appendix A. Supplementary data

Supplementary data to this article can be found online at http://dx.doi.org/10.1016/j.geoderma.2016.09.032.

References

Adamopoulos, G., Robertson, J., Morrison, N.A., Godet, C., 2004. Hydrogen content estimation of hydrogenated amorphous carbon by visible Raman spectroscopy. J. Appl. Phys. 96 (11), 6348–6352.
Antal, M.J., Grønli, M., 2003. The art, science, and technology of charcoal production. Ind. Eng. Chem. Res. 42 (8), 1619–1640.
Ascough, P.L., Bird, M.I., Francis, S.M., Thornton, B., Midwood, A.J., Scott, A.C., Apperley, D., 2011. Variability in oxidative degradation of charcoal: influence of production conditions and environmental exposure. Geochim. Cosmochim. Acta 75 (9), 2361–2378.
Ascough, P.L., Bird, M.I., Scott, A.C., Collinson, M.E., Cohen-Ofri, I., Snape, C.E., Le Manquais, K., 2010. Charcoal reflectance measurements: implications for structural characterization and assessment of diagenetic alteration. J. Archaeol. Sci. 37 (7), 1590–1599.
Ascough, P.L., Bird, M.I., Wormald, P., Snape, C.E., Apperley, D., 2008. Influence of production variables and starting material on charcoal stable isotopic and molecular characteristics. Geochim. Cosmochim. Acta 72 (24), 6090–6102.
Bergeron, S.P., Bradley, R.L., Munson, A., Parsons, W., 2013. Physico-chemical and functional characteristics of soil charcoal produced at five different temperatures. Soil Biol. Biochem. 58, 140–146.
Bird, M.I., Moyo, C., Veenendaal, E.M., Lloyd, J., Frost, P., 1999. Stability of elemental carbon in a savanna soil. Global Biogeochem. Cy. 13 (4), 923–932.
Bourke, J., Manley-Harris, M., Fushimi, C., Dowaki, K., Nunoura, T., Antal, M.J., 2007. Do all carbonized charcoals have the same chemical structure? 2. A model of the chemical structure of carbonized charcoal. Ind. Eng. Chem. Res. 46 (18), 5954–5967.
Braadbaart, F., Poole, I., van Brussel, A.A., 2009. Preservation potential of charcoal in alkaline environments: an experimental approach and implications for the archaeological record. J. Archaeol. Sci. 36 (8), 1672–1679.
Buijnsters, J.G., Gago, R., Jimenez, I., Camero, M., Agullo-Rueda, F., Gomez-Aleixandre, C., 2009. Hydrogen quantification in hydrogenated amorphous carbon films by infrared, Raman, and x-ray absorption near edge spectroscopies. J. Appl. Phys. 105 (9), 093510.
Bustin, R.M., Guo, Y., 1999. Abrupt changes (jumps) in reflectance values and chemical compositions of artificial charcoals and inertinite in coals. Int. J. Coal Geol. 38 (3–4), 237–260.
Casiraghi, C., Ferrari, A.C., Robertson, J., 2005. Raman spectroscopy of hydrogenated amorphous carbons. Phys. Rev. B 72 (8), 085401.
Cheng, C.H., Lehmann, J., Thies, J.E., Burton, S.D., Engelhard, M.H., 2006. Oxidation of black carbon by biotic and abiotic processes. Org. Geochem. 37 (11), 1477–1488.
Chia, C.H., Downie, A., Munroe, P., 2015. Characteristics of biochar: physical and structural properties. In: Lehmann, J., Joseph, S. (Eds.), Biochar for Environmental Management. Routledge, Abingdon, pp. 89–109.
Cohen-Ofri, I., Weiner, L., Boaretto, E., Mintz, G., Weiner, S., 2006. Modern and fossil charcoal: aspects of structure and diagenesis. J. Archaeol. Sci. 33 (3), 428–439.
Crawford, A.J., Belcher, C.M., 2014. Charcoal morphometry for paleoecological analysis: the effects of fuel type and transportation on morphological parameters. Appl. Plant Sci. 2 (8), 1400004.
Darmstadt, H., Pantea, D., Summchen, L., Roland, U., Kaliaguine, S., Roy, C., 2000. Surface and bulk chemistry of charcoal obtained by vacuum pyrolysis of bark: influence of feedstock moisture content. J. Anal. Appl. Pyrolysis 53 (1), 1–17.
de Lafontaine, G., Asselin, H., 2012. Soil charcoal stability over the Holocene-response to comments by Mikael Ohlson. Quat. Res. 78 (1), 155–156.

Deluca, T.H., Boisvenue, C., 2012. Boreal forest soil carbon: distribution, function and modelling. Forestry 85 (2), 161–184.
Ferrari, A.C., Robertson, J., 2004. Raman spectroscopy of amorphous, nanostructured, diamond-like carbon, and nanodiamond. Philos. Trans. R. Soc. A 362 (1824), 2477–2512.
Francioso, O., Sanchez-Cortes, S., Bonora, S., Roldan, M.L., Certini, G., 2011. Structural characterization of charcoal size-fractions from a burnt *Pinus pinea* forest by FT-IR, Raman and surface-enhanced Raman spectroscopies. J. Mol. Struct. 994 (1–3), 155–162.
Gundale, M.J., DeLuca, T.H., 2006. Temperature and source material influence ecological attributes of ponderosa pine and Douglas-fir charcoal. Forest Ecol. Manag. 231 (1–3), 86–93.
Haumaier, L., Zech, W., 1995. Black carbon - possible source of highly aromatic components of soil humic acids. Org. Geochem. 23 (3), 191–196.
Inoue, J., Inoue, Y., 2009. Comparison of the reflectances of black plant fragments in melanic Andisols with those of fresh charcoal from modern fires. Soil Sci. Plant Nutr. 55 (3), 358–362.
Inoue, J., Nishimura, R., Takahara, H., 2012. A 7500-year history of intentional fires and changing vegetation on the Soni Plateau, Central Japan, reconstructed from macroscopic charcoal and pollen records within mire sediment. Quat. Int. 254, 12–17.
Inoue, J., Okunaka, R., Kawano, T., 2016. The relationship between past vegetation type and fire frequency in western Japan inferred from phytolith and charcoal records in cumulative soils. Quat. Int. 397, 513–522.
Ishimaru, K., Hata, T., Bronsveld, P., Nishizawa, T., Imamura, Y., 2007. Characterization of sp(2)- and sp(3)-bonded carbon in wood charcoal. J. Wood Sci. 53 (5), 442–448.
Iwanami, Y., 1972. Burning temperatures of grasslands in Japan V, the comprehensive consideration on the burning temperatures 1. J. Jpn. Soc. Grassl. Sci. 18, 135–143 (in Japanese).
Jeffery, S., Bezemer, T.M., Cornelissen, G., Kuyper, T.W., Lehmann, J., Mommer, L., Sohi, S.P., van de Voorde, T.F.J., Wardle, D.A., van Groenigen, J.W., 2015. The way forward in biochar research: targeting trade-offs between the potential wins. GCB Bioenergy 7 (1), 1–13.
Jones, T.P., Scott, A.C., Cope, M., 1991. Reflectance measurements and the temperature of formation of modern charcoals and implications for studies of fusain. B. Soc. Geol. Fr. 162 (2), 193–200.
Kasin, I., Ohlson, M., 2013. An experimental study of charcoal degradation in a boreal forest. Soil Biol. Biochem. 65, 39–49.
Kawakami, M., Karato, T., Takenaka, T., 2005. Structure analysis of coke, wood charcoal and bamboo charcoal by Raman spectroscopy and their reaction rate with CO_2. ISIJ Int. 45 (7), 1027–1034.
Keiluweit, M., Nico, P.S., Johnson, M.G., Kleber, M., 2010. Dynamic molecular structure of plant biomass-derived black carbon (biochar). Environ. Sci. Technol. 44 (4), 1247–1253.
Lehmann, J., Gaunt, J., Rondon, M., 2006. Bio-char sequestration in terrestrial ecosystems-a review. Mitig. Adapt. Strateg. Glob. Chang. 11, 403–427.
Masiello, C.A., 2004. New directions in black carbon organic geochemistry. Mar. Chem. 92 (1–4), 201–213.
McDonald-Wharry, J., Manley-Harris, M., Pickering, K., 2013. Carbonisation of biomass-derived chars and the thermal reduction of a graphene oxide sample studied using Raman spectroscopy. Carbon 59, 383–405.
Mcparland, L.C., Collinson, M.E., Scott, A.C., Steart, D.C., Grassineau, N.V., Gibbons, S.J., 2007. Ferns and fires: experimental charring of ferns compared to wood and implications for paleobiology, paleoecology, coal petrology, and isotope geochemistry. PALAIOS 22 (5), 528–538.
Nara Prefecture, 1973. Land-classification Map (Soil Map of Nara Prefecture). Economic Planning Agency, Tokyo.
Nara Prefecture, 1986. Soil Map of Ueno and Nabari (Fundamental Land Classification Survey, 1:50,000). Nara Prefecture, Nara.
Nichols, G.J., Cripps, J.A., Collinson, M.E., Scott, A.C., 2000. Experiments in waterlogging and sedimentology of charcoal: results and implications. Palaeogeogr. Palaeocl. 164 (1–4), 43–56.
Nishimura, S., Fujitake, N., Hiradate, S., Shindo, H., 2012. Physicochemical and spectroscopic characteristics of charred plant fragments in Japanese volcanic ash soils. Soil Sci. 177 (12), 695–700.
Ohlson, M., 2006. Soil charcoal stability over the Holocene - comment to the paper published by de Lafontaine and Asselin. Quatern. Res. v. 76, 196–200 Quat. Res. 78 (1), 2012, 154–154.
Okunaka, R., Kawano, T., Inoue, J., 2012. Holocene history of intentional fires and grassland development on the Soni Plateau, Central Japan, reconstructed from phytolith and macroscopic charcoal records within cumulative soils, combined with paleoenvironmental data from mire sediments. The Holocene 22 (7), 793–800.
Preston, C.M., Schmidt, M.W.I., 2006. Black (pyrogenic) carbon: a synthesis of current knowledge and uncertainties with special consideration of boreal regions. Biogeosciences 3 (4), 397–420.
Rumpel, C., Chaplot, V., Planchon, O., Bernadou, J., Valentin, C., Mariotti, A., 2006. Preferential erosion of black carbon on steep slopes with slash and burn agriculture. Catena 65 (1), 30–40.
Rumpel, C., Leifeld, F., Santin, C., Doerr, S., 2015. Movement of biochar in the environment. In: Lehmann, J., Joseph, S. (Eds.), Biochar for Environmental Management. Routledge, Abingdon, pp. 283–300.
Santin, C., Doerr, S.H., Kane, E.S., Masiello, C.A., Ohlson, M., de la Rosa, J.M., Preston, C.M., Dittmar, T., 2015. Towards a global assessment of pyrogenic carbon from vegetation fires. Glob. Chang. Biol. 22 (1), 1–16.
Schmidt, M.W.I., Torn, M.S., Abiven, S., Dittmar, T., Guggenberger, G., Janssens, I.A., Kleber, M., Kogel-Knabner, I., Lehmann, J., Manning, D.A.C., Nannipieri, P., Rasse, D.P., Weiner, S., Trumbore, S.E., 2011. Persistence of soil organic matter as an ecosystem property. Nature 478 (7367), 49–56.
Scott, A.C., 2000. The Pre-Quaternary history of fire. Palaeogeogr. Palaeocl. 164 (1–4), 281–329.
Scott, A.C., 2010. Charcoal recognition, taphonomy and uses in palaeoenvironmental analysis. Palaeogeogr. Palaeocl. 291 (1–2), 11–39.
Scott, A.C., Jones, T.P., 1991. Microscopical observations of recent and fossil charcoal. Microsc. Anal. 24, 13–15.
Scott, A.C., Jones, T.P., 1994. The nature and influence of fire in carboniferous ecosystems. Palaeogeogr. Palaeocl. 106 (1–4), 91–112.
Scott, A.C., Cripps, J.A., Collinson, M.E., Nichols, G.J., 2000. The taphonomy of charcoal following a recent heathland fire and some implications for the interpretation of fossil charcoal deposits. Palaeogeogr. Palaeocl. 164 (1–4), 1–31.
Smith, M.W., Dallmeyer, I., Johnson, T.J., Brauer, C.S., McEwen, J.S., Espinal, J.F., Garcia-Perez, M., 2016. Structural analysis of char by Raman spectroscopy: improving band assignments through computational calculations from first principles. Carbon 100, 678–692.
Spokas, K.A., 2010. Review of the stability of biochar in soils: predictability of O:C molar ratios. Carbon Manag. 1 (2), 289–303.
Steinbeiss, S., Gleixner, G., Antonietti, M., 2009. Effect of biochar amendment on soil carbon balance and soil microbial activity. Soil Biol. Biochem. 41 (6), 1301–1310.
Sultana, N., Ikeya, K., Shindo, H., Nishimura, S., Watanabe, A., 2010. Structural properties of plant charred materials in Andosols as revealed by X-ray diffraction profile analysis. Soil Sci. Plant Nutr. 56 (6), 793–799.
Yamauchi, S., Kurimoto, Y., 2003. Raman spectroscopic study on pyrolyzed wood and bark of Japanese cedar: temperature dependence of Raman parameters. J. Wood Sci. 49 (3), 235–240.
Yu, X.Y., Ying, G.G., Kookana, R.S., 2006. Sorption and desorption behaviors of diuron in soils amended with charcoal. J. Agric. Food Chem. 54 (22), 8545–8550.
Zickler, G.A., Smarsly, B., Gierlinger, N., Peterlik, H., Paris, O., 2006. A reconsideration of the relationship between the crystallite size L-a of carbons determined by X-ray diffraction and Raman spectroscopy. Carbon 44 (15), 3239–3246.
Zimmerman, A.R., 2010. Abiotic and microbial oxidation of laboratory-produced black carbon (biochar). Environ. Sci. Technol. 44 (4), 1295–1301.